JOURNAL OF MECHANICAL ENGINEERING AND SCIENCES
ISSN: 2289-4659 e-ISSN: 2231-8380
VOLUME 17, ISSUE 1, 2023, 9395 – 9409
DOI: https://doi.org/10.15282/jmes.17.1.2023.9.0743

RESEARCH ARTICLE

Large strain creep analysis of composite thick-walled anisotropic cylinders

Vinod K. Arya

University of North Texas at Dallas, Dallas, Texas 75241, USA
Phone: +1 9723381375

ABSTRACT - Creep analysis of a thick-walled composite anisotropic cylinder under internal pressure and considering large strains is presented. Using a threshold creep law for composite materials, expressions for stresses, strains, and strain rates are derived for several anisotropic cases. Numerical results, presented through several graphs and tables, depict the effect of anisotropy on the stress, strain, and strain rate distributions. Since for a specific type of material anisotropy described in the paper, these quantities are found to have the lowest values at the inner radius (the potential location of cylinder failure). It is concluded that by employing such an anisotropic material for the design of a thick-walled cylinder a longer service life for the cylinder may be achieved.

ARTICLE HISTORY
Received : 28th Oct. 2022
Revised : 01st Feb. 2023
Accepted : 25th Feb. 2023
Published : 23rd Mar. 2023

KEYWORDS
Creep
Composites
Large strains
Thick-walled cylinders
Anisotropy

1.0 INTRODUCTION

Creep analysis of thick-walled cylinders, encompassing different thermal and mechanical loading conditions, a wide range of creep laws, infinitesimal (small) and finite (large) strains, made of a variety of materials viz. isotropic, anisotropic, monolithic, and composite materials, and using the classical and numerical (finite-element methods), has been the subject of active investigations during last few decades. The subject has attracted the attention of many investigators due to the important and challenging applications of thick-walled cylinders in multitude of industries such as petrochemical, structural, oil and gas, pressure vessel and nuclear industries to name a few where presence of elevated temperatures, in addition to mechanical loads, makes the creep deformation a norm, not an exception. In one of the earlier studies Weir [1] presented the creep deformation analysis of thick-walled cylinders by employing both the power and the hyperbolic sine creep laws for the isothermal and radial heat flow cases. Schweiker and Sidebottom [2] consider combined internal pressure and axial load in developing a creep theory and presenting it in the form of non-dimensional design curves with applications to varying load conditions. Their work showed a good agreement of the theory with the experimental results. King and Mackie [3] performed an experimental and theoretical study of the creep of thick-walled cylinder under internal pressure and supporting its own end load. A comparison of the theoretical (numerical) results with the experimental results is also carried out in the paper. Clarke [4] investigated, both theoretically and experimentally, the redistribution of stress caused by creep in a thick-walled cylinder subjected to internal axial and thermal loads. A review of literature by Skelton and Crossland [5] summarizes the work done on the creep of thick-walled cylinders subjected to internal pressure until the year 1967. Morris [6] derives the strain-rate equations to calculate the isothermal steady-state creep of thick-walled cylinders under internal pressure that are used as heat exchangers and fuel-pin claddings. Sim and Penny [7] use a plane strain creep analysis of the thick-walled cylinder problem considering internal pressure, external surface loading, and inertia loading using the reference stress technique. The results presented graphically are usable directly in the design of thick-walled cylinders for a single or combinations of loadings. A finite-element steady-state creep analysis of a pressurized thick-walled cylinder is presented by Altenbach et al [8] in both linear and power law creep ranges. The authors conclude that for a certain range of pressure both creep laws must be considered for accurate results. Sharma et al [9] devote their paper to the thermal creep analysis of thick-walled cylinders under internal and external pressures and conclude that less compressible thick-walled cylinders provide a better alternative for design purposes than the other cylinders. It is well known that continuing deformation under creep may attain a value where the assumption of small (infinitesimal) strains becomes increasingly invalid. Based on this fact, Rimrott [10] performed a large strain creep analysis of thick-walled cylinders subjected to internal pressure and showed that the assumption of small strains leads to a prediction of wall thickness which is on the unsafe side. Bhatnagar and Arya [11] expanded the large strain creep analysis to include the effect of anisotropy on the stress, strain, and strain-rate distributions in the cylinders and showed the anisotropy of the material to have significant effect on these quantities. With an analogy to perfect plasticity, Berman and Pai [12] developed a general steady-state creep formulation for anisotropic materials and by using its reduced piecewise linear form and comparing the calculated results with the experimental results, they concluded that the material anisotropy may cause significant errors in the solutions based on the isotropic theories. Employing a piecewise linear model, Pai [13] obtained the steady-state creep solutions for a thick-walled orthotropic cylinder for three axial conditions of plane strain, closed end, and open end. This research indicated that the anisotropy of the material had a significant effect on the creep rates, which for an anisotropic cylinder may differ by an order of magnitude compared to that in an isotropic cylinder. Bhatnagar and Gupta [14] analyzed the steady-state creep behavior

*CORRESPONDING AUTHOR | **Vinod K. Arya** | ✉ vinod.arya@untdallas.edu

of an orthotropic thick-walled cylinder subjected to internal pressure for the plane stress, plane strain and generalized plane strain cases, and found that the anisotropy of the material had a significant effect on the creep response of the cylinder. A subsequent paper by Bhatnagar et al [15] analyzed the orthotropic thick-walled cylinder problem under primary creep conditions. The cylinder was assumed to be subjected to internal and external pressures and rotary inertia. They observed that an anisotropic material strong in radial direction resulted in lower effective stress and could, therefore, be beneficial for design purposes. A recent paper by Kohli et al [16] presents the large strain creep analysis using a threshold creep law. Their work indicates that the design of thick-walled cylinder based on small strains may be on the unsafe side. From the research works described in the preceding section, one may notice that the continued deformation under creep may: 1. accumulate to a value so large that the assumption of small strains becomes increasingly invalid, and 2. cause an initially isotropic material to become anisotropic. Additionally, we also know that the use of composite materials due to their light weight, enhanced strength, resistance to damage (caused by environmental and loading conditions), and stronger durability may be of significant benefit for better design and service life of the cylinders. Therefore, the research presented in this paper is directed to study the creep deformation behavior of anisotropic thick-walled cylinders made of composite materials subjected to internal pressure and undergoing large strains. This work is believed to add vital information to guide the better design of the thick-walled cylinders as to the author's best knowledge and based on literature survey, no research study incorporating all these factors simultaneously in the creep analysis of thick-walled cylinders has been performed so far. We present the necessary mathematical framework in Section 2. Results and discussions are included in Section 3. Finally, the conclusions are stated in Section 4.

2.0 MATHEMATICAL FRAMEWORK

We consider a thick-walled cylinder with inner and outer radii a and b, respectively, and subjected to internal pressure, p. The cylinder is assumed to be made of an anisotropic (orthotropic) composite material. It is also assumed that the cylinder is undergoing large (finite) strains which mandates the use of the large (finite) strain theory to analyze its creep response.

2.1 Constitutive Equations for Anisotropic (Orthotropic) Creep Theory

Following Bhatnagar and Gupta [14], the constitutive equations for orthotropic creep theory are given as follows.

$$\varepsilon_r = \frac{\varepsilon}{2\sigma}[(G+H)\sigma_r - H\sigma_\theta - G\sigma_z] \tag{1}$$

$$\varepsilon_\theta = \frac{\varepsilon}{2\sigma}\,[(H+F)\sigma_\theta - F\sigma_z - H\sigma_r] \tag{2}$$

$$\varepsilon_z = \frac{\varepsilon}{2\sigma}\,[(F+G)\sigma_z - G\sigma_r - F\sigma_\theta] \tag{3}$$

Effective stress σ defined as,

$$\sigma = \frac{1}{\sqrt{2}}[F(\sigma_\theta - \sigma_z)^2 + G(\sigma_z - \sigma_r)^2 + H(\sigma_r - \sigma_\theta)^2]^{1/2} \tag{4}$$

is related to effective strain rate $\dot{\varepsilon}$ by the equation,

$$\sigma = f(\dot{\varepsilon}) \tag{5}$$

In these equations, *F*, *G*, and *H* are anisotropic (orthotropic) material constants and the subscripts $r, \theta,$ and z refer to stress values in the radial, tangential, and axial directions, respectively. The dot over a symbol indicates its derivative with respect to time *t*.

2.2 Compatibility Equation

Let an arbitrary element of the cylinder initially situated at a radius *r* deform to a radius given by $R = r + u$, where *u* is the displacement in the radial direction, see Figure 1 (reproduced from [11].

The natural (logarithmic) radial, ε_r, and tangential, ε_θ, strains have the following expressions,

$$\varepsilon_r = ln\left(1 + \frac{du}{dr}\right) \tag{6}$$

and

$$\varepsilon_\theta = ln\left(1 + \frac{u}{r}\right) \tag{7}$$

Combining Eqs. (6) and (7) yields the compatibility equation as,

$$r\frac{\partial \varepsilon_\theta}{\partial r} = e^{(\varepsilon_r - \varepsilon_\theta)} - 1 \tag{8}$$

2.3 Equilibrium Equation

The equation of equilibrium, see [10], is given as,

$$R \cdot \frac{d\sigma_r}{dR} = 2(\sigma_\theta - \sigma_r) \tag{9}$$

2.4 Analysis

Consider the plain strain case so that the axial strain is zero and we get,

$$\sigma_z = \frac{G\sigma_r + F\sigma_\theta}{F + G} \tag{10}$$

Combining Eqs. (4) and (10) gives,

$$\sigma = \frac{1}{K}(\sigma_\theta - \sigma_r) \tag{11}$$

in which equation,

$$K = \left[\frac{2(F+G)}{FG + GH + HF}\right]^{1/2} \tag{12}$$

The condition of incompressibility is expressed as,

$$\varepsilon_r + \varepsilon_\theta + \varepsilon_z = 0 \tag{13}$$

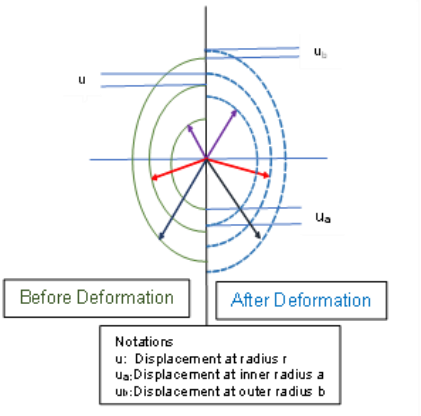

Figure 1. Cross-sections of a thick-walled cylinder

$$\varepsilon = -\frac{1}{L}\varepsilon_r = \frac{1}{L}\varepsilon_\theta \tag{14}$$

where

$$L = \left[\frac{FG + GH + HF)}{2(F+G)}\right]^{1/2} = \frac{1}{K} \tag{15}$$

Using the above equations and after some algebraic manipulations, one obtains,

$$\dot{\varepsilon} = \frac{\left(\frac{a}{r}\right)^2 \exp(2K\varepsilon_a)}{1 + \left(\frac{a}{r}\right)^2 \{\exp(2K\varepsilon_a) - 1\}} \dot{\varepsilon_a} \tag{16}$$

Eq. (16) expresses the creep strain rate, $\dot{\varepsilon}$, at any radius r as a function of creep strain rate, $\dot{\varepsilon_a}$, at the inner radius a. One also obtains the following equation

$$\frac{d\sigma_r}{d\dot{\varepsilon}} = -\frac{D}{2} \cdot \frac{\sigma}{\dot{\varepsilon}} \tag{17}$$

Eq. (17) can be integrated with the boundary conditions,

$$\sigma_r = -p \text{ at } r = a \text{ and } \sigma_r = 0 \text{ at } r = b \tag{18}$$

to yield the following integral for pressure p,

$$p = \frac{K}{2} \int_{\dot{\varepsilon_b}}^{\dot{\varepsilon_a}} \frac{\sigma}{\dot{\varepsilon}} \, d\dot{\varepsilon} \tag{19}$$

In which equation,

$$\dot{\varepsilon_b} = \frac{\left(\frac{a}{b}\right)^2 \exp(2K\varepsilon_a)}{1 + \left(\frac{a}{b}\right)^2 \{\exp(2K\varepsilon_a) - 1\}} \dot{\varepsilon_a} \tag{20}$$

and $\dot{\varepsilon_b}$ is the strain rate at the outer radius.

2.5 Stresses, Strains, and Strain Rates using Threshold Creep Law

To derive mathematical expressions for these quantities of interest, we consider a thick-walled cylinder made of Al-SiCp composite material with the anisotropic (orthotropic) behavior governed by Eqs. (1) through (5). The creep behavior of the thick-walled cylinder is described by the following creep threshold creep law used by Kohli et al [16] and Singh and Gupta [17].

$$\dot{\varepsilon} = [M(\sigma - \sigma_o)]^n \tag{21}$$

Here, M is an experimentally determined parameter, $\varepsilon, \sigma, \sigma_o, and\ n,$ respectively, denote effective creep strain, effective stress, threshold stress, and stress exponent. The dot over a symbol indicates its derivative with respect to time t. We list the values of the material constants $M,\ \sigma_o, and\ n,$ taken from [16, 17] later in the Results and Discussion section. Substituting the value of σ from Eq. (21) into Eq. (19) and integrating yields the following expression for p and,

$$p = \frac{K}{2}\left[\sigma_o\{ln(\dot{\varepsilon_a}/\dot{\varepsilon_b})\} + \frac{n}{M}\left\{\dot{\varepsilon_a}^{1/n} - \dot{\varepsilon_b}^{1/n}\right\}\right] \tag{22}$$

Using Eqs. (17), (18), (21) and (22), the following expression for the radial stress, σ_r, is obtained,

$$\sigma_r = -p + \frac{K}{2}\left[\sigma_o\{ln(\dot{\varepsilon_a}/\dot{\varepsilon})\} + \frac{n}{M}\left\{\dot{\varepsilon_a}^{1/n} - \dot{\varepsilon}^{1/n}\right\}\right] \tag{23}$$

Combining Eqs. (11) and (23) yields,

$$\sigma_\theta = -p + \frac{K}{2}\left[\sigma_o\{ln(\dot{\varepsilon_a}/\dot{\varepsilon})\} + \frac{n}{M}\left\{\dot{\varepsilon_a}^{1/n} - \dot{\varepsilon}^{1/n}\right\}\right] + K\left(\sigma_0 + \frac{\dot{\varepsilon}^{1/n}}{M}\right) \tag{24}$$

and from Eqs. (10), (23) and (24),

$$\sigma_z = -p + \frac{K}{2}\left[\sigma_o\{ln(\dot{\varepsilon_a}/\dot{\varepsilon})\} + \frac{n}{M}\left\{\dot{\varepsilon_a}^{1/n} - \dot{\varepsilon}^{1/n}\right\}\right] + \frac{F}{F+G}K\left(\sigma_0 + \frac{\dot{\varepsilon}^{1/n}}{M}\right) \tag{25}$$

Using Eq. (10) in Eqs. (1) and (2), the following expressions for the radial strain rate, $\dot{\varepsilon_r}$, and the tangential strain rate, $\dot{\varepsilon_\theta}$, result,

$$\dot{\varepsilon z_r} = \frac{\dot{\varepsilon}}{\sigma} L^2(\sigma_\theta - \sigma_r) \tag{26}$$

$$\dot{\varepsilon_\theta} = \frac{\dot{\varepsilon}}{\sigma} L^2(\sigma_r - \sigma_\theta) \tag{27}$$

and $\dot{\varepsilon}$, is given by Eq. (21).

Substituting for $\dot{\varepsilon_b}$ in terms of $\dot{\varepsilon_a}$ from Eq. (20) into Eq. (22) produces,

$$p = -\frac{K}{2}\,\sigma_0\, ln\big(X(b)\big) + \frac{Kn}{2M}\Big[1 - \big(X(b)\big)^{1/n}\Big]\,\dot{\varepsilon_a}^{1/n} \tag{28}$$

where

$$X(b) = \frac{\left(\frac{a}{b}\right)^2 \exp(2L\varepsilon_a)}{1 + \left(\frac{a}{b}\right)^2 \{\exp(2L\varepsilon_a) - 1\}} \tag{29}$$

Rearranging Eq. (28) yields,

$$\dot{\varepsilon_a} = \left(\frac{2M}{Kn}\right)^n \left[p + \frac{K}{2}\,\sigma_0\, ln\big(X(b)\big)\right]^n \cdot \left[1 - \{X(b)\}^{1/n}\right]^{-n} \tag{30}$$

Eq. (30) expresses, $\dot{\varepsilon_a}$, the strain rate at the inner radius as function of, ε_a, the strain at the inner radius. Integrating Eq. (30) with respect to time t, one obtains,

$$\left(\frac{Kn}{2M}\right)^n \int_0^{\varepsilon_a} \left[p + \frac{K}{2}\,\sigma_0\, ln\big(X(b)\big)\right]^{-n} \cdot \left[1 - \{X(b)\}^{1/n}\right]^n d\varepsilon_a = t \tag{31}$$

This equation gives the logarithmic (natural) strain ε_a as a function of time t.

3.0 RESULTS AND DISCUSSION

3.1 Material and Anisotropic Constants

For numerical computations, we consider an anisotropic thick-walled cylinder made of a composite Al-SiCp material with inner radius, a = 400 mm, outer radius, b = 800 mm, subjected to an internal pressure, p = 70.0 MPa. The values of constants for the threshold-based creep law given by Eq. (21) and taken from Kohli et al [16] and Singh and Gupta [17] are: M = 0.00227 $(sec^{-1/5}/MPa)$, $\sigma_0 = 42.56\ MPa$, and $n = 5$. To cover a wide range of anisotropy of the material, we consider five different cases with varying degrees of anisotropy. The values of the anisotropic constants for Case 1, Case 2, Case 3, and Case 4 are taken from Kulkarni et al [18]. The values for case 5 have been added by the author to cover a wider range of anisotropy in the analysis. All these values are listed in Table 1.

Table 1. Anisotropic Constants (see Ref. [18])

Ratio of anisotropic constants	G/F	H/F
Case 1	0.8159	0.6081
Case 2	1.2200	0.7452
Case 3 (Isotropic Case)	1.0000	1.0000
Case 4	0.7452	1.2200
Case 5	1.1500	1.2200

3.2 Strain Rate vs Strain Distribution

Figure 2 shows the distribution of the strain rate at the inner radius, $\dot{\varepsilon_a}$, with the strain at the inner radius, ε_a, for all five - Case 1, Case 2, Case 3 (Isotropic), Case 4, and Case 5, cases of anisotropy. It is seen from this figure that the strain rate, $\dot{\varepsilon_a}$, increases at a slow rate in the beginning of the creep deformation till the strain, ε_a, reaches a value approximately equal to 0.5. Hereafter, the strain rate, $\dot{\varepsilon_a}$, is seen to increase at a higher rate up to a value of strain, ε_a, equal to 1.0. This trend of the strain rate behavior is observed to be true for all five cases of anisotropy. The figure also depicts that the effect of anisotropy on the strain rate, $\dot{\varepsilon_a}$, is less appreciable in the earlier part of the deformation, which is until the strain at the inner radius, ε_a, attains an approximate value equal to 0.5. The effect of anisotropy is found to become increasingly more pronounced as the deformation under creep continues beyond this value of ε_a. For example, the strain rate values listed in Table 2 for ε_a = 1.0 clearly demonstrate the effect of anisotropy on the strain rate for five cases of anisotropy.

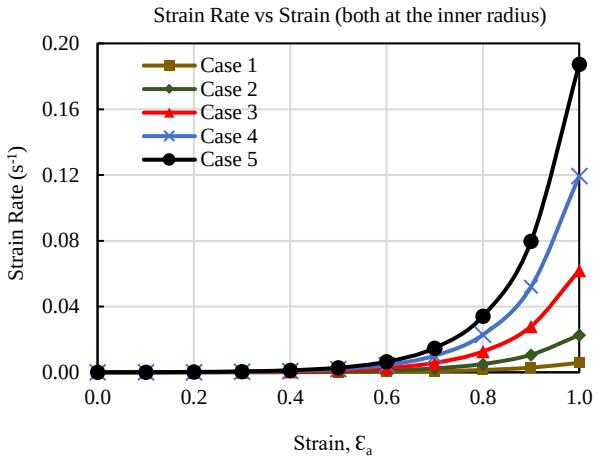

Figure 2. Strain rate, $\dot{\varepsilon_a}$, distribution with the strain, ε_a, in the thick-walled cylinder

Table 2. Values of strain rate at the outer radius of the cylinder for five cases of anisotropy

Anisotropic Case	Strain rate $\dot{\varepsilon_a}$ (s^{-1})
Case 1	5.78E-03
Case 2	2.26E-02
Case 3	6.21E-02
Case 4	1.19E-01
Case 5	1.87E-01

3.3 Strain at the Inner Radius with Time

The distribution of the strain, ε_a, at the inner radius with time is exhibited in Figure 3 for all five cases of anisotropy. It is seen that the strain at the inner radius increases with time in each case for all five cases of anisotropy. It is evident from the figure that the strain at the inner radius takes the longest time to reach the maximum value of 1.0 for Case 1 whereas the time taken for Case 5 is seen to be the shortest. The times taken for the strain to reach the maximum strain value at the inner radius for Case 2, Case 3, and Case 4 lie in between the time values for Case 1 and Case 5. In other words, the rate of deformation of the cylinder is observed to be the fastest for Case 5 and the slowest for Case 1. The deformation rates for Case 2, Case 3, and Case 4 are bounded by the rates for Case 1 and Case 5. The effect of anisotropy on the strain distribution at the inner radius of the cylinder can be more clearly observed from Table 3 which shows the times taken for the strain to reach a value equal to 1.0 for all five cases of anisotropy.

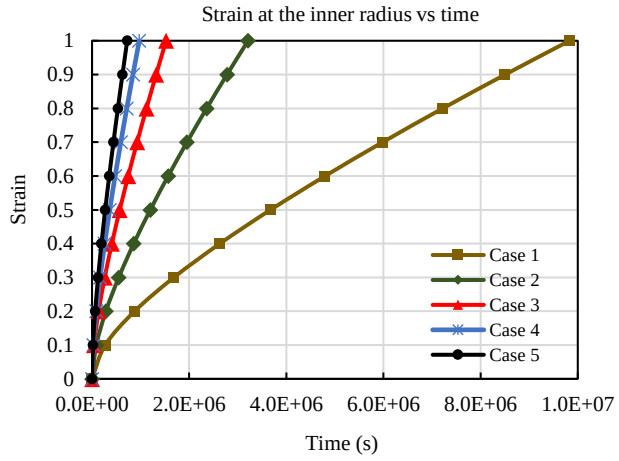

Figure 3. Distribution of the strain, $\boldsymbol{\varepsilon_a}$, at the inner radius with time for all cases of anisotropy

Table 3. Time (in seconds) taken for strain at the inner radius to reach a value of 1.0 for various cases of anisotropy

Case No.	Time (s)
Case 1	9.80E+06
Case 2	3.20E+06
Case 3	1.50E+06
Case 4	9.70E+05
Case 5	7.20E+05

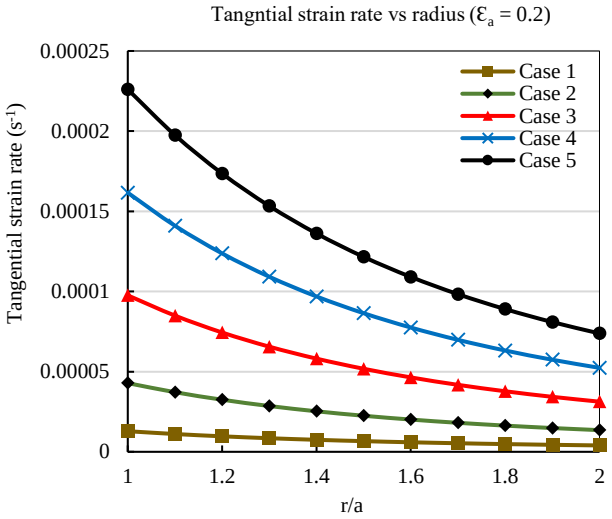

Figure 4. Tangential strain rate, $\dot{\varepsilon}_{\theta}$, distribution at various radii of the thick-walled cylinder for ε_a = 0.2 for all five cases of anisotropy

3.4 Tangential Strain Rate across the Cylinder Wall

The plots of the tangential strain rate, $\dot{\varepsilon\theta}$, with radius, for two arbitrarily chosen values of the strain at the inner radius viz. ε_a=0.2 and ε_a=0.8, are displayed in Figures 4 and 5 for all cases of anisotropy. The results, although calculated for all ε_a values from 0.0 to 1.0, are plotted only for these two values of ε_a to facilitate clear visualization of trends shown by the numerical results. It is observed from these figures, that for all cases of anisotropy, the tangential strain rate, $\dot{\varepsilon\theta}$, has a maximum value at the inner radius of the cylinder from where it falls continuously to attain a minimum value at the outer radius of the cylinder. A comparison of corresponding curves at two values of strain at the inner radius viz. ε_a=0.2 and ε_a=0.8 shows that for all anisotropic cases the tangential strain rate at all radii of the cylinder keeps increasing with the increasing values of the strain at the inner radius. One may also notice from Figures 4 and 5 that for both values of strain at the inner radius, ε_a=0.2 and ε_a=0.8, the tangential strain rate, $\dot{\varepsilon\theta}$, has the highest values for Case 5 and the lowest values for Case 1. The values for Cases 2, 3, 4 are bounded by the values for Cases 1 and 5. Comparing the corresponding curves for the anisotropic cases, it can be clearly noticed that the effect of anisotropy on the tangential strain rate becomes increasingly more pronounced with the increasing deformation (strain) under creep. The values listed in Table 4 for the tangential strain rate at the inner radius for two values of strain, ε_a=0.2 and ε_a=0.8, and for all five cases of anisotropy clearly reveal this trend.

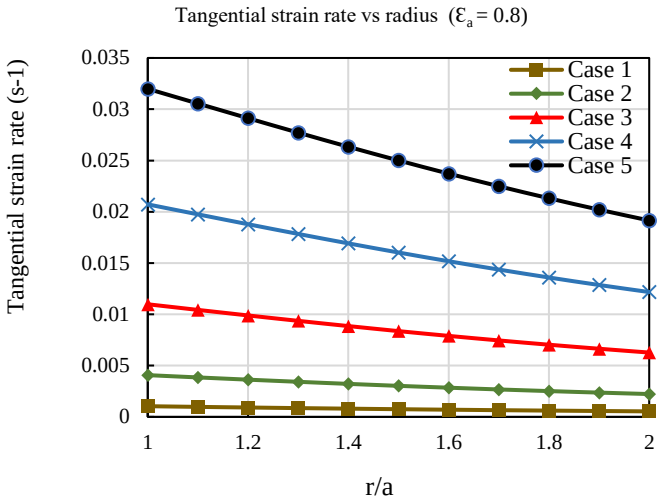

Figure 5. Tangential strain rate, $\dot{\varepsilon}_{\theta}$, distribution at various radii of the thick-walled cylinder for ε_a = 0.8 for all five cases of anisotropy

Table 4. Tangential strain rate at inner radius for two values of strain at the inner radius, $\varepsilon_a = 0.2$ and $\varepsilon_a = 0.8$, for all cases of anisotropy

Strain at the Inner Radius		0.2	0.8
Tangential strain rate, (s^{-1})	Case 1	1.28E-05	1.04E-03
	Case 2	4.28E-05	4.07E-03
	Case 3	9.76E-05	1.09E-02
	Case 4	1.60E-04	2.07E-02
	Case 5	2.26E-04	3.20E-02

3.5 Radial Stress Distribution

The radial stress distribution in the wall of the thick-walled cylinder is exhibited in Figure 6 for all five cases of anisotropy and for two values of the strain at the inner radius viz. $\varepsilon_a = 0.2$ and $\varepsilon_a = 0.8$. It is observed that the anisotropy of the material has minimal influence on the radial stresses in the cylinder at all stages of deformation.

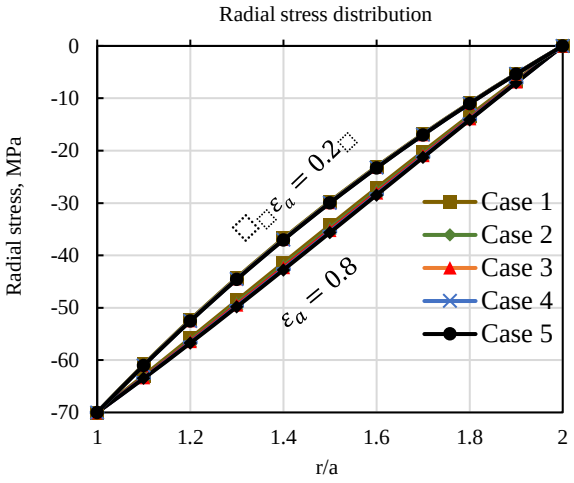

Figure 6. Radial stress distribution at various radii of cylinder for all cases of anisotropy and strain values $\varepsilon_a = 0.2$ and $\varepsilon_a = 0.8$.

3.6 Tangential Stress Distribution

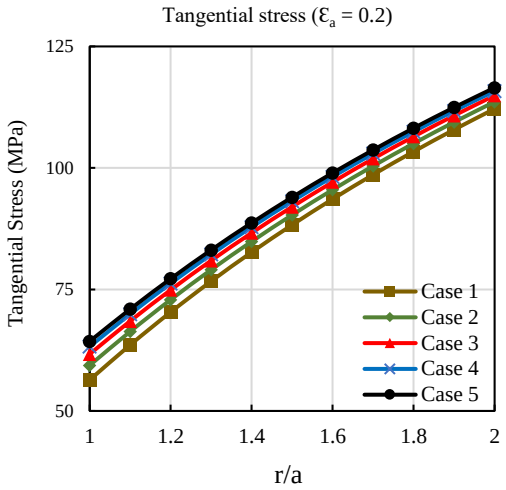

Figure 7. Tangential stress at various radii of cylinder for all cases of anisotropy and strain value $\boldsymbol{\varepsilon_a = 0.2}$.

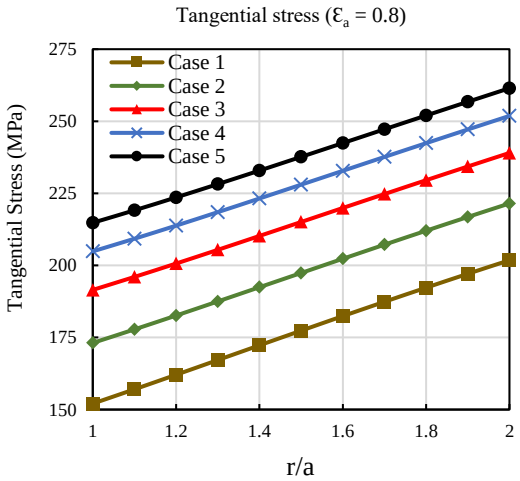

Figure 8. Tangential stress at various radii of cylinder for all cases of anisotropy and strain value $\boldsymbol{\varepsilon_a = 0.8}$

However, this difference in tangential stress values becomes more noticeable as the deformation (strain) under creep continues, for example, for strain value $\varepsilon_a = 0.8$.

Table 5. Tangential stress at outer radius for two values of strain $\boldsymbol{\varepsilon_a}$ for all cases of anisotropy

Strain at the Inner Radius, ε_a		0.2	0.8
Tangential stress (MPa) at the outer radius	Case 1	112.17	201.80
	Case 2	113.61	221.49
	Case 3	114.90	239.01
	Case 4	115.82	251.86
	Case 5	116.50	261.46

3.7 Effective Stress Distribution with Radius

The distribution of effective stress, σ, at different radii of the thick-walled cylinder for all five anisotropic cases is shown in Figure 9. The figure exhibits the effective stress distribution at two stages of deformation viz. $\varepsilon_a = 0.2$ and $\varepsilon_a = 0.8$. The figure shows that for both values of strain ε_a and for all cases of anisotropy the effective stress has the highest (maximum) value at the inner radius, and it decreases continuously with increasing radius to attain the lowest (minimum) value at the outer radius. It is further observed that the effective stress values at all radii and for both strain values, $\varepsilon_a = 0.2$ and $\varepsilon_a = 0.8$, are the highest for Case 5 and the lowest for Case 1. The values for Cases 2, 3, and 4 are bounded by these highest and lowest values for Case 5 and Case 1, respectively. To clearly judge the effect of anisotropy on the effective stress values at the inner radius, the potential failure location of the thick-walled cylinder, we list these

values in Table 6 for $\varepsilon_a = 0.2$ and $\varepsilon_a = 0.8$. It is interesting to note, from Table 6, that the effective stress at the inner radius has the lowest value for Case 1 among all five anisotropic cases.

Since the inner radius is the potential location of the failure of the cylinder, the use of a composite cylinder made of a material possessing the anisotropic properties as described in Case 1 may result in a longer life for the thick-walled cylinder.

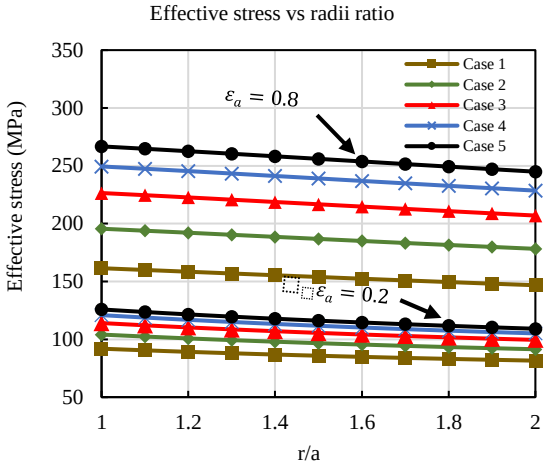

Figure 9. Effective stress at various radii of the cylinder for all cases of anisotropy and strain values $\boldsymbol{\varepsilon_a = 0.2}$ and $\boldsymbol{\varepsilon_a = 0.8}$

Table 6. Effective stress at the inner radius for two values of $\boldsymbol{\varepsilon_a}$ for all cases of anisotropy

Strain at the Inner Radius, ε_a		0.2	0.8
Effective stress (MPa) at the inner radius	Case 1	91.90	161.47
	Case 2	104.11	195.61
	Case 3	114.06	226.47
	Case 4	120.92	249.53
	Case 5	125.83	266.77

3.8 Effective Stress Distribution with Time

A more comprehensive effect of anisotropy on the effective stress distribution in the thick-walled cylinder can be seen in Figure 10. The figure displays the effective stress distribution at the inner radius of the cylinder with time for all five cases of anisotropy. The effective stress and time values cover the strain at the inner radius (ε_a) values from 0.0 to 1.0 (not shown in the figure). It is noticed from Table 7 that at the inner radius, the highest effective stress occurs for Case 5 and has a value equal to 357.69 MPa whereas the minimum effective stress occurs for Case 1 with a value equal to 199.75 MPa. The highest effective stress values for Cases 2, 3, and 4 are found to be 249.03 MPa, 295.22 MPa, and 330.53 MPa, respectively. Analyzing the effective stress vs time curves in Figure 10, one may easily infer that the rate of increase of the effective stress is the highest for Case 5 and the lowest for Case 1. Table 7 below gives the detailed information about the rates of increase of effective stress from its initial value to the maximum value for all cases of anisotropy when the cylinder deforms from the initial strain value of $\varepsilon_a = 0.0$ to the final strain value of $\varepsilon_a = 1.0$.

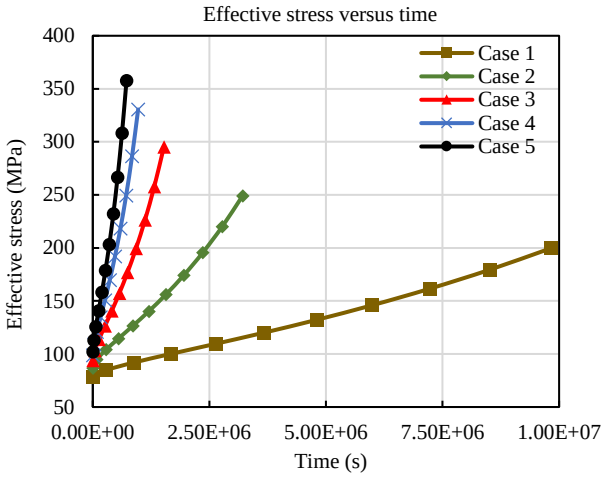

Figure 10. Plot of effective stress at the inner radius with time for all cases of anisotropy

Table 7. Time for the maximum effective stress at the inner radius for all cases of anisotropy

Anisotropic Case	Stress (MPa)	Time (s)
Case 1	199.75	9.80E+06
Case 2	249.03	3.20E+06
Case 3	295.22	1.50E+06
Case 4	330.53	9.70E+05
Case 5	357.69	7.20E+05

3.9 Effective Stress Distribution with Radius

The distribution of effective stress, σ, at different radii of the thick-walled cylinder for all five anisotropic cases is shown in Figure 9. The figure exhibits the effective stress distribution at two stages of deformation viz. $\varepsilon_a = 0.2$ and $\varepsilon_a = 0.8$. The figure shows that for both values of strain ε_a and for all cases of anisotropy the effective stress has the highest (maximum) value at the inner radius, and it decreases continuously with increasing radius to attain the lowest (minimum) value at the outer radius. It is further observed that the effective stress values at all radii and for both strain values, $\varepsilon_a = 0.2$ and $\varepsilon_a = 0.8$, are the highest for Case 5 and the lowest for Case 1. The values for Cases 2, 3, and 4 are bounded by these highest and lowest values for Case 5 and Case 1, respectively. To clearly judge the effect of anisotropy on the effective stress values at the inner radius, the potential failure location of the thick-walled cylinder, we list these values in Table 6 for $\varepsilon_a = 0.2$ and $\varepsilon_a = 0.8$. It is interesting to note, from Table 6, that the effective stress at the inner radius has the lowest value for Case 1 among all five anisotropic cases.

Since the inner radius is the potential location of the failure of the cylinder, the use of a composite cylinder made of a material possessing the anisotropic properties as described in Case 1 may result in a longer life for the thick-walled cylinder.

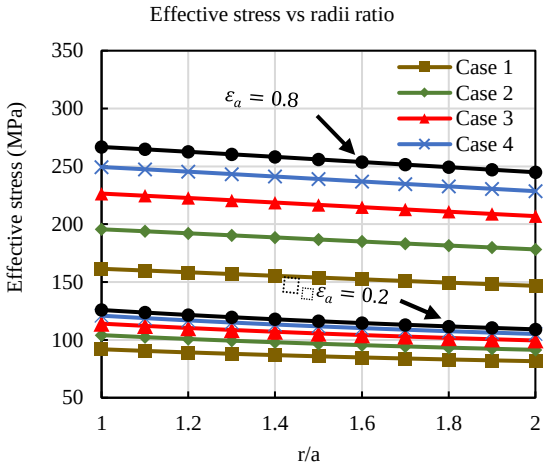

Figure 9. Effective stress at various radii of the cylinder for all cases of anisotropy and strain values $\boldsymbol{\varepsilon_a = 0.2}$ and $\boldsymbol{\varepsilon_a = 0.8}$

Table 6. Effective stress at the inner radius for two values of $\boldsymbol{\varepsilon_a}$ for all cases of anisotropy

Strain at the Inner Radius, ε_a		0.2	0.8
Effective stress (MPa) at the inner radius	Case 1	91.90	161.47
	Case 2	104.11	195.61
	Case 3	114.06	226.47
	Case 4	120.92	249.53
	Case 5	125.83	266.77

3.10 Effective Strain-Rate Distribution with Radius

The effective strain rate distribution, for all cases of anisotropy, is exhibited in Figures 11 and 12 for two strain values at the inner radius viz. $\varepsilon_a = 0.2$ and $\varepsilon_a = 0.8$, respectively. It is seen from these figures that the effective strain rate decreases from the highest value at the inner radius to the lowest value at the outer radius at both stages of deformation. It is also seen that at both stages of deformation (strain at the inner radius) the effective strain rate has the highest value for Case 5, which then keeps reducing from Case 4 to Case 3 to Case 2 and Case 1 (the lowest) values. Since the effective strain rate at the inner radius governs the service life of the thick-walled cylinder, it is expedient to list in Table 8, the effective strain rate values at the inner radius for all cases of anisotropy and at these two stages of deformation, $\varepsilon_a = 0.2$ and $\varepsilon_a = 0.8$.

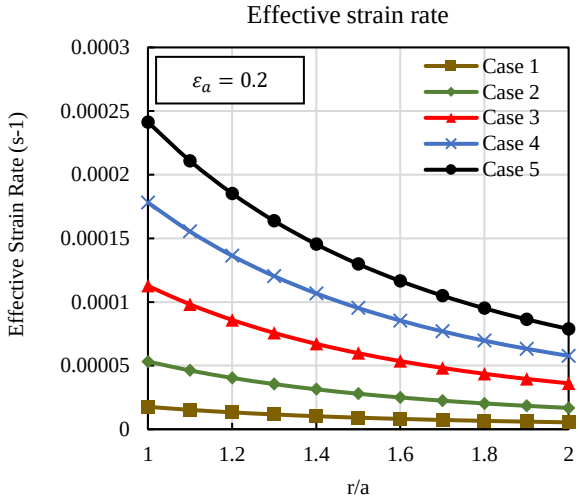

Figure 11. Effective strain rate distribution at different radii for $\boldsymbol{\varepsilon_a = 0.2}$ for all cases of anisotropy

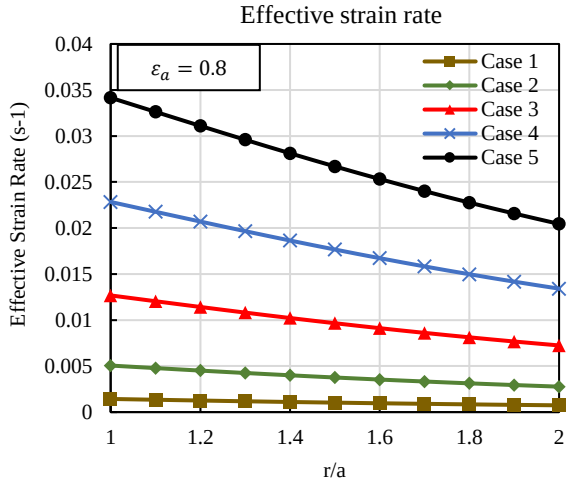

Figure 12. Effective strain rate distribution at different radii for $\boldsymbol{\varepsilon_a = 0.8}$ for all cases of anisotropy

The effect of anisotropy can be clearly seen from this table which depicts the highest effective strain rates for Case 5 and the lowest for Case 1. Since the strain rate values for Case 1 are lower than that for the isotropic case (Case 3); the advantage achieved by using a composite material with an anisotropy of type defined in Case 1 as compared to an isotropic material in the design of thick-walled cylinders, is self-evident.

Table 8. Effective strain rate at the inner radius at two stages of deformation ($\boldsymbol{\varepsilon_a = 0.2}$ and $\boldsymbol{\varepsilon_a = 0.8}$) for all cases of anisotropy

Anisotropic Case		$\varepsilon_a = 0.2$	$\varepsilon_a = 0.8$
Case 1	Effective Strain Rate, $\dot{\varepsilon}$, (s^{-1})	1.76E-05	1.41E-03
Case 2		5.32E-05	5.06E-03
Case 3		1.13E-04	1.20E-02
Case 4		1.78E-04	2.28E-02
Case 5		2.00E-04	3.41E-02

3.11 Effective Strain-Rate Distribution with Time

The distribution of the effective strain at the inner radius with time for five cases of anisotropy is shown in Figure 13. The time values displayed in the figure correspond to the strain at the inner radius, ε_a, ranging from 0.0 to 1.0. It is seen that the effective strain rates at the inner radius increase continuously with time for all anisotropic cases. The strain rates for all cases of anisotropy increase continuously as the time (or deformation under creep) progresses. It is important to note that the effective strain rate at the inner radius has the highest value for Case 5 and the lowest for Case 1, and the effective strain rate values for Cases 2, 3, and 4 are bounded by the values for Case 1 and Case 5. A more comprehensive and concise idea about the trends shown in Figure 13 can be had from Table 9 which shows the highest values of the effective strain rates at the inner radius and the corresponding times for all cases of anisotropy. The values listed are when the strain at the inner radius, ε_a, has attained a value equal to 1.0. Table 9 shows that the effective strain rates for Case 1 and Case 2 are lower, and for Case 4 and Case 5, they are higher than that for Case 3 (isotropic case). We also notice from the table that the time taken to reach the highest strain rates are larger for Case 1 and Case 2, and they are smaller for Case 4 and Case 5 than that for Case 3 (isotropic case). In other words, lower strain rates and larger times than those for Case 3 (which defines an isotropic cylinder) are obtained for Case 1 and Case 2 (which define orthotropic cylinders).

From Tables 3, 7 and 9, one can clearly see that the use of a material with the anisotropic properties as defined in Case 1, results in the lowest strain, lowest effective stress, lowest effective strain rate and the longest time to reach the maximum deformation stage (defined by $\varepsilon_a = 1.0$) of the cylinder. Since these values of effective stress, effective strain rate, and time are the values at the inner radius of the cylinder, which is the most likely location of the cylinder failure, it may be concluded that using an anisotropic material with Case 1 type anisotropy may be beneficial for the design of thick-walled cylinders for industrial applications as this may yield longer service lives for the cylinders.

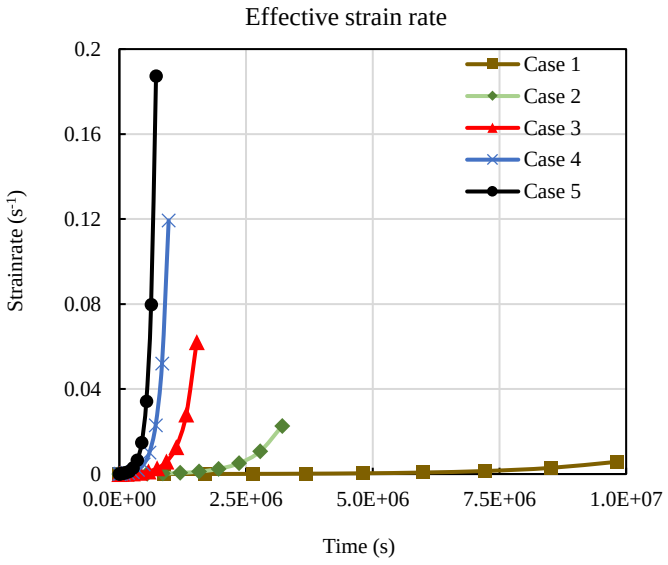

Figure 13. Plot of effective strain rate at the inner radius with time for all cases of anisotropy

Table 9. Effective strain rates at the inner radius and the corresponding times for all cases of anisotropy

Anisotropic Case	Strain rate (s^{-1})	Time (s)
Case 1	5.70E-03	9.80E+06
Case 2	2.30E-02	3.20E+06
Case 3 (isotropic case)	6.20E-02	1.50E+06
Case 4	1.20E-01	9.70E+05
Case 5	1.90E-01	7.20E+05

4.0 CONCLUSIONS

This paper presents the steady-state creep analysis of composite thick-walled cylinders subjected to internal pressure. The composite cylinder's material is assumed to be anisotropic (orthotropic) and it is supposed to be undergoing large (finite) creep deformation (strains). The threshold creep law proposed by Kohli et al. and Singh and Gupta is employed to derive the mathematical expressions for stress, strain and strain rate distributions in the anisotropic (orthotropic) cylinder by employing the orthotropic theory of creep presented by Bhatnagar and Gupta. Five anisotropic cases, to cover a wide range of anisotropy of the material, have been considered in the analysis. Numerical computations for stresses, strains and strain rates for all five anisotropic cases have been performed, and the results to show the distribution of these quantities with the radius of the cylinder and time have been presented through several tables and graphs. It is seen from these results that the anisotropy of the material has significant effect on the stress, strain, and strain rate distributions for each of the five anisotropic cases considered in this work. The most important result brought forward by the present research establishes that for an anisotropic material of type as defined in Case 1, the effective strain, effective stress and the effective strain rates at the inner radius have significantly lower values than the corresponding values for the isotropic material define by Case 3 (the isotropic case). Since the most potential location of the failure of the cylinder is at its inner radius, the lower values of the effective strain, effective stress and the effective strain rate for Case 1 type anisotropic material than the corresponding values for Case 3 at this location lead to the conclusion that the use of Case 1 type anisotropic material, instead of an isotropic material, in the design of the thick-walled cylinders may be beneficial and result in a longer service life for the cylinder.

5.0 ACKNOWLEDGMENTS

The author did not receive any financial support to perform or publish this research work.

6.0 NOMENCLATURE

ε	Strain
σ	Stress
r	Radius
R	Deformed Radius
u	Radial Displacement
a	Inner Radius
b	Outer Radius
p	Internal Pressure
M	Experimentally Determined Parameter
σ_0	Threshold Stress
n	Exponent in Creep Law
F, G, H, L, K	Anisotropic Constants
Subscripts	
r, θ, z	Denote Radial, Tangential, and Axial Directions, respectively
a, b	Denote Quantities at Inner and Outer Radius, respectively

7.0 REFERENCES

[1] C. D. Weir, "The creep of thick tubes under internal pressure," *Applied Mechanics Division Summer Conference*, The American Society of Mechanical Engineers, Berkeley, California, June 13-15, 1957.

[2] J. W. Schweiker and O. M. Sidebottom, "Creep of thick-walled cylinders subjected to internal pressure and axial load," *Experimental Mechanics,* vol. 5, pp. 186-192, 1965.

[3] R. H. King and W. W. Mackie, "Creep of thick-walled cylinders*," Journal of Fluids Engineering,* vol. 89, no. 4, pp. 877 – 884, 1967.

[4] J. M. Clarke, "An investigation of stress redistribution caused by creep in a thick-walled circular cylinder subjected to axial and thermal loading," *Ministry of Technology, Aeronautical Research Council*, No. 1024, 1969.

[5] W. J. Skelton and B. Crossland, "Creep of thick-walled cylinders subjected to internal pressure: Review of literature*," Proceedings of the Institution of Mechanical Engineers*, vol. 182, no. 3, pp. 132 – 138, 1967.

[6] R. E. Morris, "Strain-rate equations for calculation of secondary creep deformation of thick-walled tubes with internal or external pressure*," NASA Technical Memorandum,* TM X-2339, 1971.

[7] R. G. Sim and R. K. Penny, "Plane strain creep behaviour of thick-walled cylinders," International Journal of Mechanical Sciences, *v*ol. 13, pp. 987-1009, 1971.

[8] H. Altenbach, K. Gorash and K. Naumenko, "Steady-state creep of a pressurized thick cylinder in both the linear and the power law ranges," *Acta Mechanica*, vol. 195, pp. 263-274, 2008.

[9] R. Sharma, S. Sharma, and Z. Radakovic, "Thermal Creep Analysis of pressurized thick-walled cylindrical vessels," *Structural Integrity and Life*, vol. 18, pp. 7-14, 2018.

[10] F. P. J. Rimrott, "Creep of thick-walled tubes under internal pressure considering large strains," *Journal of Applied Mechanics,* vol. 26, pp. 271-275, 1959.

[11] N. S. Bhatnagar and V. K. Arya, "Large strain creep analysis of thick-walled cylinders," *International Journal of Non-Linear Mechanics,* vol. 9, pp. 127-140, 1974

[12] I. Berman and D. H. Pai, "A theory of anisotropic steady-state creep," *International Journal of Mechanical Sciences*, vol. 8, pp. 341-352. 1966.

[13] D. H. Pai, "Steady-state creep analysis of thick-walled orthotropic cylinders," *International Journal of Mechanical Sciences,* vol. 9, pp. 335-348, 1967.

[14] N. S. Bhatnagar and S. K. Gupta, "Analysis of thick-walled orthotropic cylinder in the theory of creep," *Journal of the Physical Society of Japan.* vol. 27, pp. 1655-1661, 1969.

[15] N. S. Bhatnagar, P. Kulkarni. and V. K. Arya, "Analysis of an orthotropic thick-walled cylinder under primary creep conditions," *International Journal of Pressure Vessels and Piping,* vol. 23, no. 3, pp. 165-185, 1986.

[16] G. S. Kohli, T. Singh, and H. Singh, "Creep analysis in thick composite cylinder considering large strains*," Journal of the Brazilian Society of Mechanical Sciences and Engineering,* vol. 42, pp. 68, 2020.

[17] T. Singh, V. K. Gupta, "Effect of material parameters on steady state creep in a thick composite cylinder subjected to internal pressure," *Journal of Engineering Research*, vol. 6, no. 2, pp. 20-32, 2009.

[18] P. S. Kulkarni, N. S. Bhatnagar, and V. K. Arya, "Creep analysis of thin-walled anisotropic cylinders subjected to internal pressure, bending and twisting*," Proceedings of the Workshop on Solid Mechanics*, India, March 13-16, 1985.